Experimental study of a twin-rotor axial-flow turbine for wave energy conversion

Tiago Belo Cardoso Marques
tiago.b.marques@tecnico.ulisboa.pt
Instituto Superior Técnico, Universidade de Lisboa, Portugal

November, 2020

Given the oscillating behaviour of waves, the extraction of their energy requires the use of turbines either with symmetrical geometries, so that performance is independent of the direction of flow, or capable of being equipped with flow rectifying systems. The turbine studied in this thesis offers a solution of the second type. The use of two rotors coupled to the same shaft is proposed. Through an annular valve, made possible by the innovative diffusor geometry, the air flux is oriented alternately to only one of the rotors, allowing for the use of turbine blades optimized for unidirectional flow. Due to the symmetry, of the model, the study is made with only one rotor.

The work consists in the construction of an axial stator and rotor set and associated structures, and their experimental testing.

The performance curves are determined, dimensionlessly representing the pressure, power and efficiency drop as a function of the flow. The aerodynamic losses estimated for the rotor to which the flow has been cut are subtracted to the calculated power, making the adjustment to the global efficiency.

Additionally, traverses are made at the entrance and exit of the rotor, which provide information about the speed and direction of the flow. Using these, the performance of the rotor is analyzed and the losses in each section of the turbine are estimated.

Finally, the results are compared with the computational project of the blades and with the previously studied radial configuration of the turbine.

I. Introduction

The search for alternatives to fossil fuels as energy sources has lead to the interest in different renewable energy sources, among which wave energy.

The wave power in coastal areas has been estimated at 2TW [1]. As a point of reference the worldwide power consumption was 2.4TW in 2017 [2]. While a large part of this might not be profitably exploitable, it may be of ecological and strategical interest in some high wave power density coastlines as well as in remote offshore applications.

The first use of wave energy conversion into electric power was implemented in ocean signalling buoys by Yoshio Masuda [3]. These worked on the principle of the Oscillating Water Column [OCW]. Instead of the turbine being submerged, the oscillating water surface creates an alternating pressure between ends of the turbine. These are still the most widely employed wave energy converting mechanisms [4].

Due to the oscillating nature of the air flow, unidirectional turbines are not adequate since they would not work in reverse flow conditions. A possible solution is to employ self-rectifying turbines, i.e., turbines whose geometry, usually symmetrical, allows them to work in either direction. Two of the most popular solutions of this type are the *Wells* turbine and the Impulse

type turbine (Fig. 1).

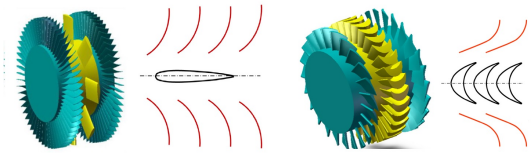

(a) *Wells* Turbine (b) Impulse Turbine

Figure 1: *3D models and respective blade schemes for typical self-rectifying turbines (Reproduced from [4])*

The *Wells* rotor employs a symmetrical airfoil laid along the rotor symmetry plane. While the rotor has an inherently low drag and consequentially a high peak efficiency, the blades are susceptible to steep angles of attack which will induce flow separation. This results in a steep efficiency decline for high flow rates. This could be a hindrance for OCW applications, which deal with highly varying conditions.

The impulse or action type turbine relies on the change of the direction of the flow instead of a fall in pressure. While having a higher drag and lower efficiency, this does not suffer from the sudden loss typical of *Wells* rotors.

The bi-radial turbine proposed in [5] and tested in [6] offers a novel approach to action turbines with both radial inlet and outlet. This achieved a maximum efficiency of 79%, possibly the highest ever achieved by a self-rectifying turbine.

A different approach to the oscillation problem is to introduce an active system of rectifying valves external to the blades themselves. This enables the use of more efficient turbines optimized for unidirectional flow. These systems usually involve a higher degree of complexity and hence a higher cost of production and maintenance.

An attempt to simplify the rectification systems was proposed in [7]. The novelty in the system consists in the spider shaped diffuser. By stacking two diffusers against each other, an annular shaped valve can slide from one to the other moving only a minimum distance (Fig. 2). The simplicity of the mechanism may greatly reduce associated costs and should enable a quick toggle (in the order of tenths of second) [8].

The diffuser geometry is detailed in [9].

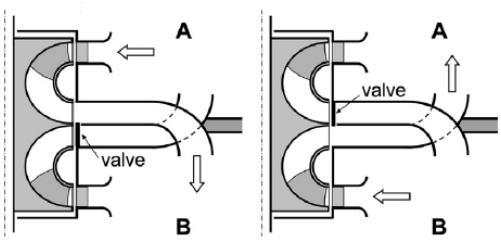

Figure 2: *Axially sliding cylindrical valve system for twin-rotor turbines (Reproduced from [8])*

Two versions of the twin-rotor turbine were originally proposed: one with radial rotors and one with axial rotors. The first of these configurations was tested in [10]. The second, the axial configuration is the object of study of the present dissertation. For this purpose an axial rotor and stator were designed in [11] through a computation fluid dynamics [CFD] analysis. The current thesis also aims at validating the performance estimated for the blades.

II. Experimental Setup

i. Project and construction

The test rig at the turbo-machinery laboratory in Instituto Superior Técnico [IST] was used for all tests. A schematic representation of the rig and the model built may by seen in Figure 3.

The flow enters the turbine through a reverse elliptical inlet, which helps avoid separation at the inlet section. A cylindrical cover shields the flow from the irregular shapes of the torque meter and power generator/electrical motor.

The guide vanes at the stator deflect the incoming airflow to an adequate angle of attack β_3 for the moving rotor blades (Figure 11). These, in turn, extract energy from the flow.

Downstream from the rotor, a cylindrical section exists, both for structural reasons and to facilitate measurements, particularly traverses, in this section.

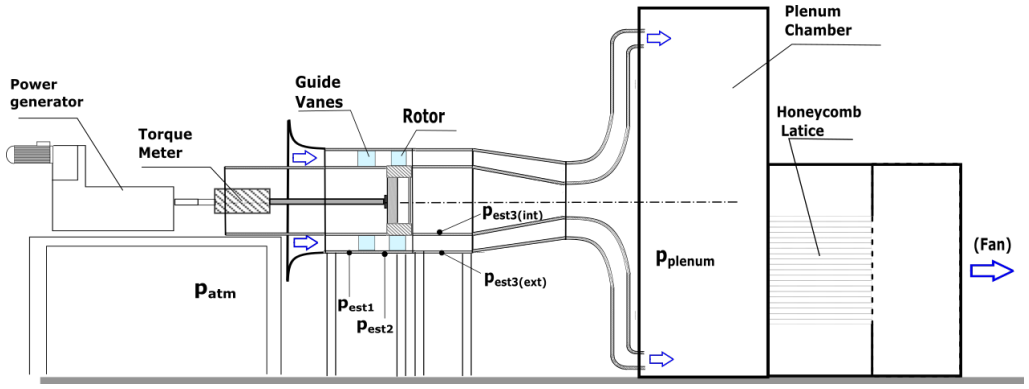

Figure 3: *Schematic representation of the test rig*

The "spider" diffuser having been produced for the previously tested radial version of the twin-rotor turbine, its dimensions were inadequate for the built shroud. A conical nozzle allows for the use of the turbine model with the pre-existing diffuser. The spider diffuser then slows the flow leading to a plenum chamber. Here the air is assumed to be at null velocity, whereby the static pressure equals the stagnation pressure.

A honeycomb lattice joins the plenum chamber to an outlet nozzle, minimizing *swirl* (air movement in the circumferential direction), and smoothing any disturbances that might propagate upstream from the fan. The test rig is driven by the variable speed fan at the exit that imposes a lower than atmospheric pressure to the plenum.

The rotor and stator were built according to the geometry detailed in the original computational study ([11]). The general dimensions are presented on Table 1. To achieve these dimensions while maintaining the geometric relations, a 19 blade stator was used, along with a 40 blade rotor.

An additional rotor with 21 blades was built to test the influence of the number of blades on the performance of the turbine. For this purpose, the geometry of individual blades was maintained and a spacer was placed between each two. The rotors are henceforth referred to as **R40** and **R21** according to the number of blades.

D_{ext}	500 mm
D_{int}	340 mm
Axial chord (Rotor)	81,9 mm
Axial chord (Stator)	83,9 mm
Rotor-Stator distance	40 mm
Stator exit angle α_2	35°

Table 1: *Model dimensions*

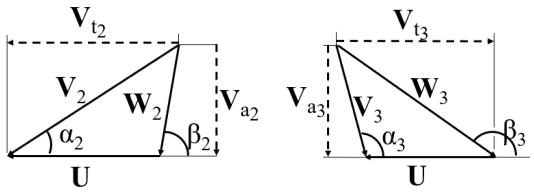

(a) Rotor inlet (b) Rotor exit

Figure 4: *Velocity triangles in an axial flow turbine*

Figure 4 shows typical velocity triangles for axial flow turbines. For the reaction degree of 50% for which the blades were designed, the triangles are symmetrical. These were also designed for a 90° angle of attack β_2 at maximum efficiency, which theoretically corresponds to an exit angle α_3 of 90°.

ii. Instrumentation and Data Acquisition

To measure the turbine power output, a torque meter was used. This instrument allowed for si-

multaneous acquisition of rotating speed. The readings were passed on as voltage output to a digital data acquisition system.

The specific mass of air ρ may be calculated given the temperature and atmospheric pressure (Equation 1). Air humidity was not taken into account for these measurements, since its has negligible effect on air density at room temperature ($< 1\%$ at $20°\mathrm{C}$, $1\ \mathrm{atm}$). Temperature was measured using a bulb thermometer ($\epsilon_\mathrm{T} = \pm 0{,}25°\mathrm{C}$), while the atmospheric pressure was measured using a digital barometer ($\epsilon_{\mathrm{p_{atm}}} = \pm 300\mathrm{Pa}$).

$$\rho = \frac{\mathrm{p_{atm}}}{\mathrm{R(T + 273.15)}} \tag{1}$$

where $\mathrm{p_{atm}}$ is the atmospheric pressure in Pa, T is the dry temperature in $°\mathrm{C}$ and $\mathrm{R} = 287{,}06\ \mathrm{J.kg^{-1}.K^{-1}}$ is the air specific constant for ρ in $\mathrm{kg.m^{-3}}$.

The remaining pressure readings were made using pressure transducers, again returning voltage outputs to be digitally processed. The calibration of the transducers was done manually using a *Betz* manometer to extract the curves relating the voltage outputs to the pressures imposed.

Compounding the uncertainty inherent to the calibration with that of the sensors, these had an error of approximately $0{,}5\%$ of the readings.

The pressure at the rotor exit $\mathrm{p_{est_3}}$ is the simple average of the pressure at the hub and the shroud. Such was not possible at the rotor inlet, due to physical constraints. Here, the pressures $\mathrm{p_{est_1}}$ and $\mathrm{p_{est_2}}$ are assumed to be equal to the pressure measured at the shroud.

A cylindrical directional probe was used for the traverse tests. At the tip, the probe has 2 lateral holes symmetrically positioned relative to a central hole. The pressure difference between the lateral holes increases with the incidence angle of the flow. The pressure difference between the lateral holes and the centre increases with the velocity of the flow. Calibration tests returned the relationship between these values, enabling the determination of flow velocity and direction.

The cylindrical probe was mounted on a traversing system. This allowed for the vertical (radial) movement of the probe through the different turbine sections. A further movement permits the rotation of the probe around its axis, so as to change the angle of incidence of the flow. Both movements were driven by stepper motors, themselves controlled using a microcontroller connected to the computer, while the probe holes were connected to the data acquisition system through the aforementioned pressure transducers.

The loop thus created facilitated a precise direction determination through the null method, i.e., the iterative angular movement of the probe until meeting the flow at a $0°$.

Finally, a calibration was done, relating the total flow rate to the static pressure $\mathrm{p_{est_2}}$. For this purpose, traverses with a *Pitot* tube were executed along the inlet section. The stagnation pressure readings returned a velocity curve. Assuming axial symmetry, this was then integrated (Eq. 2) and related to $\mathrm{p_{est_2}}$ (Eq. 3).

$$\mathrm{Q} = \int_0^{2\pi} \int_{\mathrm{r_{int}}}^{\mathrm{r_{ext}}} \mathrm{V_{a_i}} \mathrm{r dr d}\theta \tag{2}$$

$$\mathrm{Q} = \sqrt{\frac{\mathrm{p_{est2}}}{\rho \times 120{,}5}} \tag{3}$$

where Q is the flow-rate in $\mathrm{m^3 s^{-1}}$ and $\mathrm{p_{est2}}$ is in Pa.

III. Experimental Results

i. Drag and Friction Torque

The first tests performed were meant to determine the friction losses of the rotor bearings and other rotating parts. The results were then further divided into dry friction - due to bearings and sliding contacts on the rotor or shaft, and aerodynamic drag intrinsic to the blades. The former is dependant on the present construction, and was thus added to any readings, as is does not relate to the turbine concept itself. The latter is inherent to the blades and thus not discounted. Since it was determined with zero flow rate (the fan exit was sealed) it

corresponds to the drag necessarily induced by the passive rotor on a twin-rotor assembly, therefore becoming essential to describing the twin-rotor turbine performance ahead.

Dry friction was assumed to be constant and aerodynamic drag to be dependant on the second power of the rotation speed (Eq. 4). Hence, friction was measured both by directly measuring the torque when varying rotation speed and indirectly estimated by readings of the turbine freely decaying its rotation from a speed of 1000 r.p.m. to a halt.

The tests produced different results, though within the same order of magnitude. The direct measurement having been assumed as more accurate, those results were used henceforth.

$$\mathrm{T_a} = \mathrm{T_{a_{dry}}} + \mathrm{t_{a_{aero}}}\Omega^2 = 9{,}64 \times 10^{-5}\Omega^2 + 0{,}057 \tag{4}$$

where T is the torque in Nm and Ω, the rotation speed in $\mathrm{rad.s^{-1}}$.

ii. Overall performance

The following dimensionless quantities allow for a general characterization of the turbine performance.

$$\Phi = \frac{\mathrm{Q}}{\Omega.\mathrm{D}^3} \tag{5}$$

$$\Pi = \frac{\mathrm{T}}{\rho.\Omega^2\mathrm{D}^5} \tag{6}$$

$$\Psi = \frac{\mathrm{p_{atm}} - \mathrm{p_{plenum}}}{\rho.\Omega^2\mathrm{D}^2} \tag{7}$$

Where Φ is the flow-rate coefficient; Q, the flow-rate [$\mathrm{m^3/s}$]; Ω, the rotating speed [$\mathrm{rad/s}$]; D, the turbine diameter [m]; Π, the power coefficient; T, the Torque [N.m]; ρ , the specific mass of air [$\mathrm{kg/m^3}$]; Ψ, the pressure coefficient [*adim.*].

Figures 5 and 6 present the dimensionless coefficients for power and pressure.

The power supplied to the generator P [W], may be calculated from the torque T [Nm] and rotation speed Ω [rad.s] (Eq. 8).

$$\mathrm{P} = \mathrm{T}\Omega \tag{8}$$

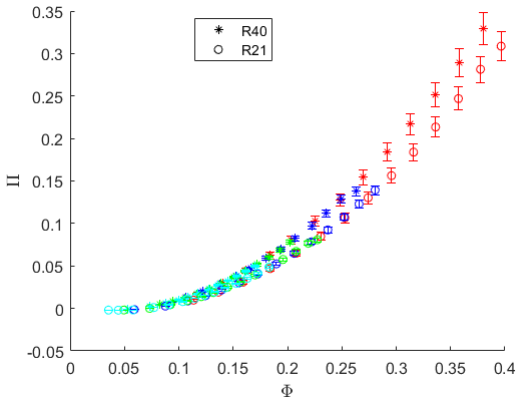

Figure 5: *Power coefficient versus flow-rate coefficient*
R40: $\Pi = 2{,}645\phi^2 - 0{,}132\phi - 0{,}00286$
R21: $\Pi = 2{,}501\phi^2 - 0{,}214\phi + 0{,}00286$

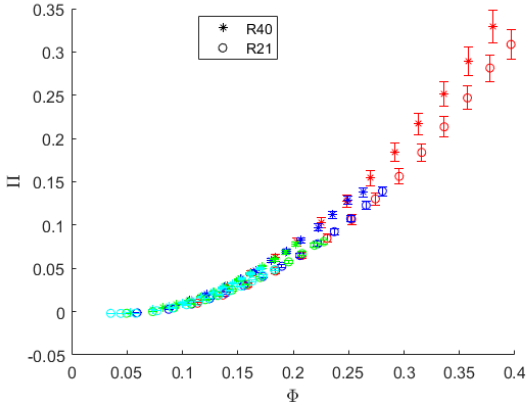

Figure 6: *Pressure coefficient versus flow-rate coefficient*
R40: $\Psi = 20{,}46\phi^2 - 0{,}837\phi + 0{,}0339$
R21: $\Psi = 16{,}46\phi^2 - 1{,}068\phi + 0{,}0550$

The overall efficiency of the model being tested ($\eta_{\mathrm{ts_{(turbine)}}}$) can be expressed as a ratio of the power supplied to the generator and the total pressure fall between the atmosphere at the inlet and the plenum chamber (Eq. 9).

A further quantity can be similarly defined as the efficiency of the model up to the rotor exit $\eta_{\mathrm{ts_{(rotor)}}}$ (Eq. 10). The calculated values for $\eta_{\mathrm{ts_{(turbine)}}}$ and $\eta_{\mathrm{ts_{(rotor)}}}$ are shown in the graphs of Figures 7 and 8 respectively.

$$\eta_{\mathrm{ts_{(turbine)}}} = \frac{\mathrm{P}}{\mathrm{Q}(\mathrm{p_{atm}} - \mathrm{p_{plenum}})} = \frac{\Pi}{\Psi\Phi} \tag{9}$$

$$\eta_{ts_{(rotor)}} = \frac{P}{Q(p_{atm} - p_3)} \tag{10}$$

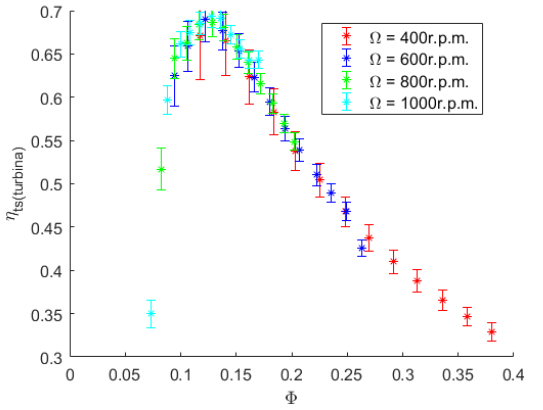

Figure 7: *Turbine efficiency versus flow-rate coefficient for* ***R40***

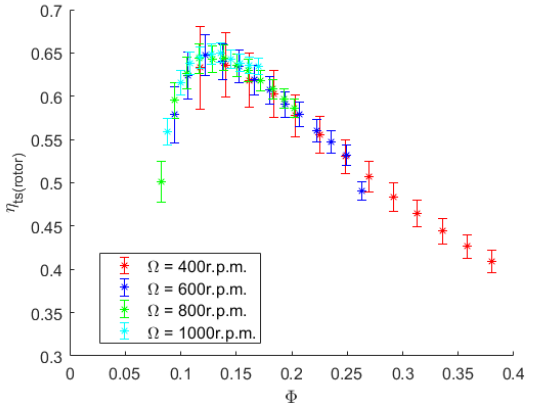

Figure 8: *Rotor efficiency versus flow-rate coefficient for* ***R40***

The difference between $\eta_{ts_{(turbine)}}$ and $\eta_{ts_{(rotor)}}$ corresponds to the increased performance gained by the use of the diffuser. By reducing the static pressure drop, it allows for a greater amount of energy to be extracted for the same pressure drop. In the present model, this value is negative for the greater flow rates, whence the diffuser must be inducing losses instead of recuperating energy. The phenomenon is discussed further on below.

Finally, subtracting the estimated torque losses originating from the passive rotor, an approximation of the twin-rotor turbine efficiency can be calculated. This is presented in Figure 9.

Rotor	*Rotor*		*Turbine*		*Twin Rotor*	
	$\Phi_{\eta max}$	η_{max}	$\Phi_{\eta max}$	η_{max}	$\Phi_{\eta max}$	η_{max}
R40	0,15	0,65	0,12	0,69	0,14	0,61
R21	0,15	0,60	0,12	0,67	0,16	0,60

Table 2: *Total-static efficiency η_{ts} peak values (600r.p.m.)*

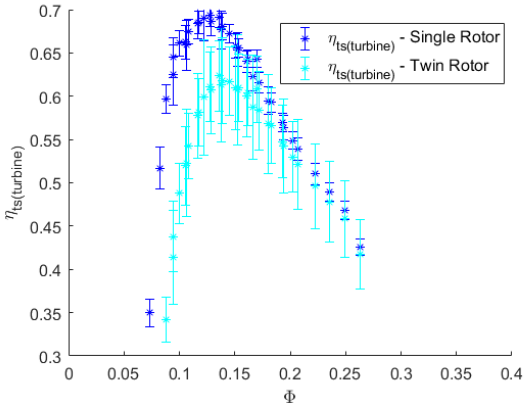

Figure 9: *Twin Rotor Turbine efficiency versus flow-rate coefficient for* ***R40***

The calculated efficiencies are condensed in Table 2, where peak efficiency values are presented.

iii. Traverses

Following the determination of the overall turbine performance, an attempt is made to characterize the flow in each section of the model. For this purpose, radial traverses were done both at the rotor inlet and exit.

At the rotor inlet, the traverses characterize the deflection produced by the guide vanes. Since these are static relative to the probe support, the trials were performed at 5 different circumferential positions downstream of a single blade. The assumption of axial symmetry

then allowed for extrapolation of the results to the full circumference of the stator.

Deflection angle values were averaged along the radial coordinate (Equation 11), the angles being weighted according to their contribution to the total flow rate. The mean absolute flow angle $\overline{\alpha_2}$ for each circumferential position is presented in Figure 10.

$$\overline{\alpha} = \frac{\int_{r_{int}}^{r_{ext}} V_a \alpha r dr}{\int_{r_{int}}^{r_{ext}} V_a r dr} \tag{11}$$

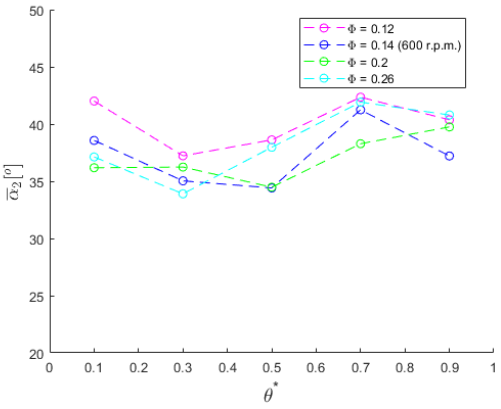

Figure 10: *Absolute flow angle (α_2) averaged along the radial path for each circumferential position*

In Figures 11 and 12 the results of the radial traverses are shown in the form of velocity triangles for ease of analysis.

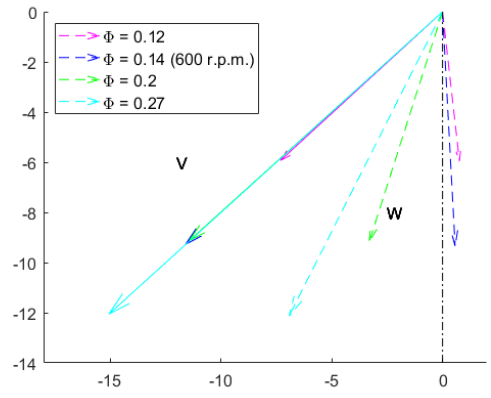

Figure 11: *Absolute (V) and Relative (W) velocities at rotor inlet* [m/s] *for* ***R40***

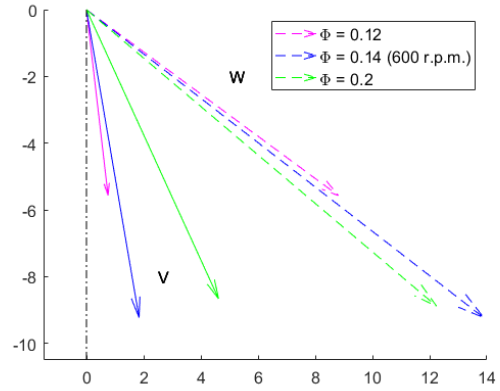

Figure 12: *Absolute (V) and Relative (W) velocities at rotor exit* [m/s] *for* ***R40***

iv. Losses

The same weighting principle used for the mean angles may be applied to calculate a mean stagnation pressure (Eq. 12) for each section.

$$\overline{p_{0_i}} = \frac{\int_0^{2\pi} \int_{r_{int}}^{r_{ext}} V_{a_i} p_{0_i} r dr d\theta}{\int_0^{2\pi} \int_{r_{iytnt}}^{r_{ext}} V_{a_i} r dr d\theta} \tag{12}$$

The stagnation pressure coefficients Λ_i (Eqs. 13, 14 and 15) help locate the sources of stagnation pressure losses. The coefficients represent the percentage of the flow's total energy lost in the corresponding section. Note that the remainder percentage corresponds to the turbine's total-static efficiency, i.e. the percentage not lost in either section. The relationship is clear in Figure 13.

$$\Lambda_{atm-2} = \frac{Q(p_{atm} - \overline{p_{0_2}})}{Q(p_{atm} - p_{pleno})} = \frac{\overline{p_{0_2}}}{p_{pleno}} \tag{13}$$

$$\Lambda_{2-3} = \frac{(\overline{p_{0_2}} - \overline{p_{0_3}})Q - T\Omega}{Q(p_{atm} - p_{pleno})} \tag{14}$$

$$\Lambda_{3-pleno} = \frac{Q(\overline{p_{0_3}} - p_{pleno})}{Q(p_{atm} - p_{pleno})} = \frac{\overline{p_{0_3}}}{p_{pleno}} - 1 \tag{15}$$

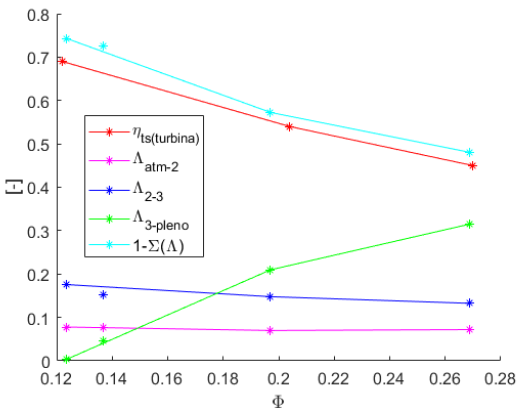

Figure 13: *Loss coefficients and turbine efficiency versus flow-rate coefficient*

To assist the assessment of the geometry of the blades, a blade loss coefficients λ were calculated. These relate total pressure losses to the kinetic energy in the flow in the axial direction.

$$\lambda_{\text{atm}-2} = \frac{\text{p}_\text{A} - \overline{\text{p}_{0_2}}}{\frac{1}{2}\rho\overline{\text{V}_\text{a}}^2} \tag{16}$$

$$\lambda_{2-3} = \frac{\overline{\text{p}_{0_2}} - \overline{\text{p}_{0_3}}}{\frac{1}{2}\rho\overline{\text{V}_\text{a}}^2} \tag{17}$$

The coefficients are then compared with those calculated through the *Soderberg* correlation $\xi_{\text{Soderberg}}$ detailed in [12]. Table 3 includes the calculated coefficients and the corresponding $\xi_{\text{Soderberg}}$ estimated as well as the adjusted (converted to absolute velocity) coefficient for direct comparison.

Stator	$\lambda_{\text{atm}-2}$	$\lambda_{\text{atm}-2}\sin^2(\alpha_2)$	$\xi_{\text{Soderberg(atm}-2)}$
	0,42	0,14	0,080
R40	λ_{2-3}	$\lambda_{2-3}\sin^2(\beta_3)$	$\xi_{\text{Soderberg}(2-3)}$
	1,03	0,32	0,16
R21	λ_{2-3}	$\lambda_{2-3}\sin^2(\beta_3)$	$\xi_{\text{Soderberg}(2-3)}$
	1,03	0,38	0,14

Table 3: *Blade loss coefficients for $\eta_{\text{ts}_{\text{max}}}$ and Soderberg estimates*

Given the ideal nature of the estimates, the magnitude of the deviations was considered reasonable. The higher loss coefficients for the **R21** rotor were not expected and no explanation was found for these.

v. Total-total efficiency η_{tt}

Besides the previously calculated total-static efficiencies, the total-total efficiency η_{tt} of the turbine was calculated. This comprises only the guide vanes and rotor and corresponds to the efficiency supposing the use of the total stagnation pressure at the exit, usually only relevant for a multi-stage turbine. This is therefore not significant to the current use of the designed blades, and serves only the purpose of fully characterizing the turbine.

$$\eta_{\text{tt}} = \frac{\text{P}}{(\overline{\text{p}_{0_2}} - \overline{\text{p}_{0_3}})\text{Q}} \tag{18}$$

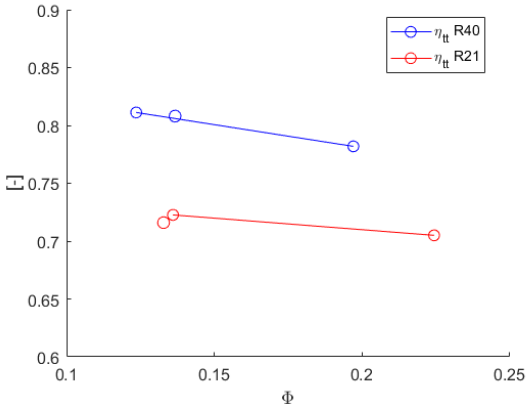

Figure 14: *Total-total rotor efficiency*

The values determined for η_{tt} are shown in the graph in Figure 14. A total-total efficiency of $\eta_{\text{tt}_{\text{max}}} = 0{,}81$ was achieved with **R40**, while **R21** only reached $\eta_{\text{tt}_{\text{max}}} = 0{,}72$.

vi. Comparisons

The CFD project [11] had predicted a maximum efficiency of $\eta_{\text{tt}_{\text{max}}} = 0{,}90$ for **R40**. While the current results do not appear to reject this, when error inducing factors are considered, they are not sufficient to validate the study.

For comparison with the radial configuration, a further quantity, the efficiency of the diffuser, is introduced, allowing for the determination of the influence of the diffuser in the efficiency of the turbine.

$$\epsilon_0 = \frac{\mathrm{p_{plenum}} - \mathrm{p_3}}{\frac{1}{2}\rho\overline{\mathrm{V_{a_3}}}^2} \tag{19}$$

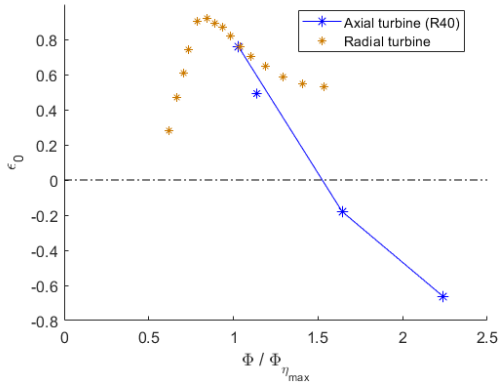

Figure 15: *Diffuser efficiency ϵ_0 (Radial data from [10])*

Figure 15 shows the diffuser efficiency values for both configurations of the twin-rotor turbine. In the original radial twin-rotor turbine, the diffuser acted favourably, recuperating kinetic energy. In the current experiment, this did not prove so for the higher flow rates. The negative values of diffuser efficiency point to it contributing to the turbine losses instead of alleviating them. Whereas ideally it would decelerate the flow and increase the static pressure, it ends up adding a considerable pressure drop, resulting in an overall higher $\mathrm{p_{atm}} - \mathrm{p_{plenum}}$ static pressure differential, i.e., a lower performance for the same imposed differential.

While its use is still indispensable given the importance of the rectifying sliding valve, the geometry should have been better adapted to the new configuration, mainly by reconsidering the conical coupling and possibly adjusting the opening curvature, thereby minimizing the zones with high propensity for flow separation.

In Figure 16, the total-static efficiency calculated for the twin-rotor (**R40**) is presented alongside the analogous values for the Radial twin-rotor turbine, as well as reference values for both *Wells* and impulse type turbines.

Compared to the reference values for the *Wells* and Impulse turbines, the current turbine exhibits a compromise between those, having a higher peak efficiency than the impulse turbine and a wider plateau in the flow rate dependency than the Wells turbine with its sudden drop. The impulse turbines slower efficiency decay for higher flow rates when compared to the twin-rotor turbines might be related to the latter's sharply curved diffuser. This is offset by the increased efficiency in using higher efficiency unidirectional blades. The *Wells* turbine sharp decrease in efficiency has to do with the flow separation for high flow rates.

Despite performing arguably better than either of these self rectifying solutions, in comparison with the Radial Twin-rotor configuration previously tested, the present model fares poorly in both metrics.

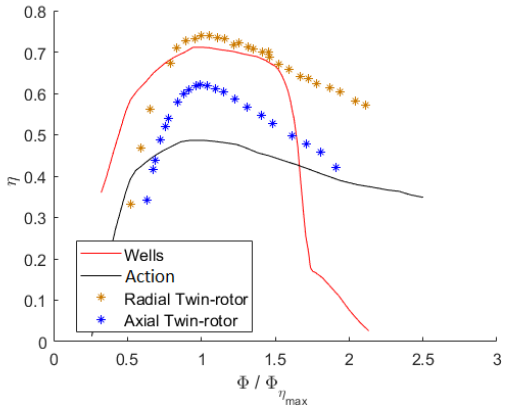

Figure 16: *Total-static efficiency η_{ts} comparison for different turbines*

IV. Conclusions

The aim of the thesis was the testing of the axial configuration of the twin rotor turbine.

A second rotor, **R21**, with 21 blades was built for testing the influence of the number of blades on the rotor performance. As expected the originally designed **R40** rotor showed a higher overall total-total efficiency η_{tt} which

translates to a higher maximum turbine efficiency $\eta_{\mathrm{ts}_{\max}}$. However, the efficiency curve **R21** overcomes the **R40** efficiency for higher flow rates. No explanation was found for this reason, though the tests for multiple rotation speeds, along with the coincidence of η_{ts} curves reached through the traverses (Fig. 13) do not suggest invalid data.

The experiment revealed a lower total-total efficiency for the **R40** rotor than the one predicted by the CFD analysis. The magnitude of the difference is not negligible, and the tests alone do not confidently validate the design. Nevertheless, it is not so large as to invalidate it either.

A global twin-rotor efficiency $\eta_{\mathrm{ts}_{(\mathrm{twin})}} = 0{,}61$ was achieved. This presented a good compromise between the *Wells* and Action turbines. However, the turbine did not perform adequately when compared to the previously tested radial twin-rotor turbine [10], its only advantage being for higher absolute flow rates and specific speeds. Furthermore, the axial version is the least compact of the two.

Further tests in variable flow conditions are required to fully describe the turbine.

References

[1] K. Gunn and C. Stock-Williams. Quantifying the global wave power resource. Renewable Energy, Elsevier, 44:296–304, 2012. doi:10.1016/j.renene.2012.01.101.

[2] *Global Energy & CO2 Status Report 2017*. International Energy Agency, 2018.

[3] Y. Masuda and M. E. McCormick. *Experiences in pneumatic wave energy conversion in Japan*. Utilization of Ocean Waves - Wave to Energy Conversion, Amer. Soc. Civil Eng., 1986.

[4] A. F. Falcão and J. C. C. Henriques. Oscillating-water-column wave energy converters and air turbines: A review. Renewable Energy. Elsevier, 85:1391–1424, 2016. doi:10.1016/j.renene.2015.07.086.

[5] L. Gato and A. Falcão. *Turbine with Radial Inlet and Outlet Flow Rotor for use in Bi-directional Flows*. World Patent WO/2011/102746, 2011.

[6] A. A. D. Carrelhas, A. R. Maduro, L. M. C. Gato, J. C. C. Henriques, and A. F. O. Falcão. Performance of the self-rectifying biradial air turbine with fixed guide vanes arranged into concentric annular rows. Energy, Elsevier, 198:117211, 2020. doi:10.1016/j.energy.2020.117211.

[7] A. F. O. Falcão, L. M. C. Gato, and J. C. C. Henriques. *Air turbine for applications in wave energy conversion*. World Patent WO/2014/185806, 2014.

[8] A. F. O. Falcão, L. M. C. Gato, J. C. C. Henriques, J. E. Borges, B. Pereiras, and F. Castro. A novel twin-rotor radial-inflow air turbine for oscillating-water-column wave energy converters. Energy, Elsevier, 93:2116–2125, 2015. doi:10.1016/j.energy.2015.10.046.

[9] J. T. Q. Melo. *Projeto do difusor de uma turbina tetra-radial auto-retificadora*. Tese de Mestrado, Instituto Superior Técnico, 2016.

[10] B. S. C. Lopes. *Construção e ensaio de um modelo de turbina de ar auto-retificadora de rotor duplo para sistemas de aproveitamento da energia das ondas*. Tese de Mestrado, Instituto Superior Técnico, 2017.

[11] A. C. L. Paralta. *Projeto de uma Turbina de Rotor Duplo Axial com Válvulas Auto-retificadoras para Conversores de Energia das Ondas*. Tese de Mestrado, Instituto Superior Técnico, 2017.

[12] A. F. O. Falcão. *Sebenta de Turbomáquinas*. Associação de estudantes do Instituto Superior Técnico, 2017.